Cyclic Shear Behavior of Concrete-Filled Composite Plate Shear Wall Components with Bolted Splices

Jia-Hau Liu[1] and Michel Bruneau, Dist.M.ASCE[2]

Abstract: The composite plate shear walls/concrete-filled (C-PSW/CF) system consists of steel faceplates with concrete infill sandwiched between them. This structural system has garnered international attention, generating interest for its use in nonseismic regions with bolted splices. This paper investigates the shear behavior of C-PSW/CF components with bolted splices through experimental tests and finite-element analyses. Six shear tests were conducted on different splice details, and results were compared with the finite-element models. The study found that AISC strength equations conservatively estimate the ultimate strength of the splices. Additionally, four more finite-element models explored shear behavior in longer wall scenarios. A new formula was proposed to calculate shear strength when the splice is governed by the bearing. This study provides experimental and analytical insights into the shear behavior of bolted C-PSW/CF components.
DOI: 10.1061/JSENDH.STENG-14408.

Author keywords: Composite plate shear wall/concrete filled (C-PSW/CF); Bolted splices; Cyclic tests; Finite element analysis.

Introduction and Background

The composite plate shear wall/concrete-filled (C-PSW/CF) system, alternatively referred to as SpeedCore, is a structural element comprising two steel faceplates with a concrete core sandwiched between them. The steel plates are connected by tie bars or steel-headed stud anchors, both of which are embedded within the concrete infill. This wall system has demonstrated its efficiency in accelerating construction timelines, as evidenced by its successful implementation in the Rainier Square Tower project in Seattle. In recent years, extensive research has been conducted to explore and understand the behavior, analysis, and design of the C-PSW/CF system. Various studies have focused on the in-plane flexural and shear behavior of these walls (Agrawal 2020; Alzeni 2014; Alzeni and Bruneau 2017; Kizilarslan 2021; Kizilarslan and Bruneau 2021, 2023; Sener and Varma 2014; Shafaei et al. 2021; Varma et al. 2014). The results from these tests and analyses have been summarized and implemented in ASCE-7 (ASCE 2022), AISC 360 (AISC 2022b), and AISC 341(AISC 2022a).

The general attention that recent implementations of this wall system in high-rises in seismic regions has received has subsequently sprung interest for implementation where wind design governs over seismic regions, such as Boston, New York, and Miami. In many of these regions, contractors typically prefer bolted splices over welded splices for field applications. This paper presents the results of research to investigate the shear behavior of C-PSW/CF components with bolted splices.

In the design of bolted splices, multiple limit states are considered. The more ductile limit states of slip-critical resistance, net and gross section yielding strengths, and bearing strength are deemed preferable in bolted C-PSW/CF components as they are relatively more ductile than others. Regarding the bearing strength, previous research (Brown et al. 2007; Frank and Yura 1981; Kim and Yura 1996; Kulak et al. 1987; Lewis and Zwememan 1996) has demonstrated that the bearing strength of $2.4dtF_u$ can typically be achieved when the bolt hole develops a 6.4-mm (0.25-in.) deformation. Further research (Kim and Lee 2020; Može 2018) has explored the limits of bearing-type connections, finding that larger end distances or bolt spacings result in higher bearing strengths. However, an upper limit of $3.0dtF_u$ is commonly adopted for most cases even when the hole is allowed to develop a substantially greater than 6.4-mm (0.25-in.) elongation.

While the structural behavior of all-steel bolted connections has been previously investigated, the focus here is on the shear behavior of bolted C-PSW/CF components. Fig. 1 shows an elevation from a 28-story SpeedCore project in Boston featuring bolted splices, designed by Magnusson Klemencic Associates (MKA). The figure highlights horizontal and vertical bolted splices. Generally, the horizontal splices are expected to be governed by their flexural strength, meaning they are primarily designed to resist tension and compression forces induced by the overturning moment at both ends. In contrast, the vertical splices are designed to resist shear flow between the wall segments, as shown in Fig. 2. These vertical splices typically run the height of the wall, and testing here is performed on a segment of that entire length.

The shear specimens were designed to investigate shear behavior and applicability of AISC 360 equations for C-PSW/CF with bolted splices. Three limits states, bearing, slip-critical, and yielding, were analyzed to study the shear behavior of these connections. Additionally, these specimens were tested without the concrete infill to contrast behavior of all-steel connections with the comparable noncomposite connections.

Six shear component tests were conducted, alongside corresponding finite-element models. Eccentricity typically exists in a shear splice, which can introduce torsion in a bolt group system. However, as the splice length increases, as is the case in a wall, this eccentric effect tends to become negligible. To study the effects of

[1]Graduate Research Assistant, Dept. of Civil Structural and Environmental Engineering, Univ. at Buffalo, Buffalo, NY 14260 (corresponding author). ORCID: https://orcid.org/0009-0003-9608-1932. Email: jiahauli@buffalo.edu

[2]SUNY Distinguished Professor, Dept. of Civil Structural and Environmental Engineering, Univ. at Buffalo, Buffalo, NY 14260. ORCID: https://orcid.org/0000-0003-1170-468X. Email: bruneau@buffalo.edu

Note. This manuscript was submitted on August 28, 2024; approved on March 24, 2025; published online on July 16, 2025. Discussion period open until December 16, 2025; separate discussions must be submitted for individual papers. This paper is part of the ***Journal of Structural Engineering***, © ASCE, ISSN 0733-9445.

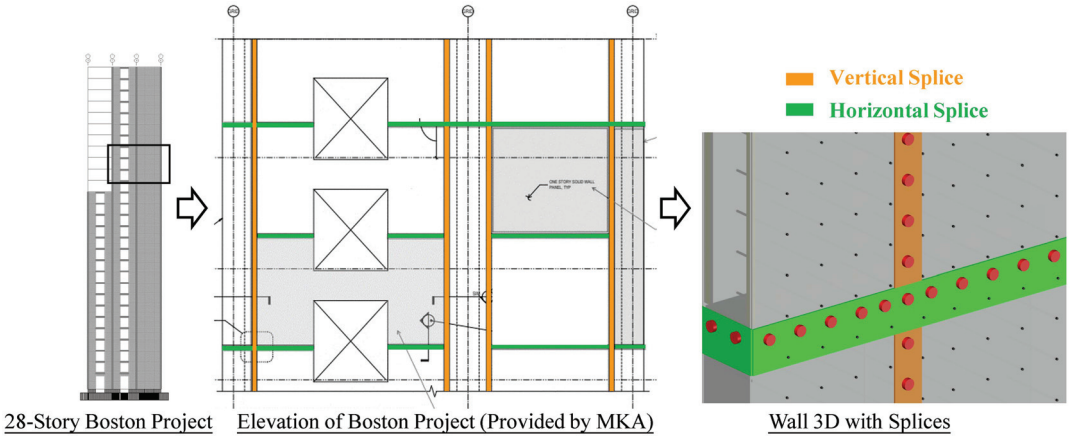

Fig. 1. 28-story Boston project.

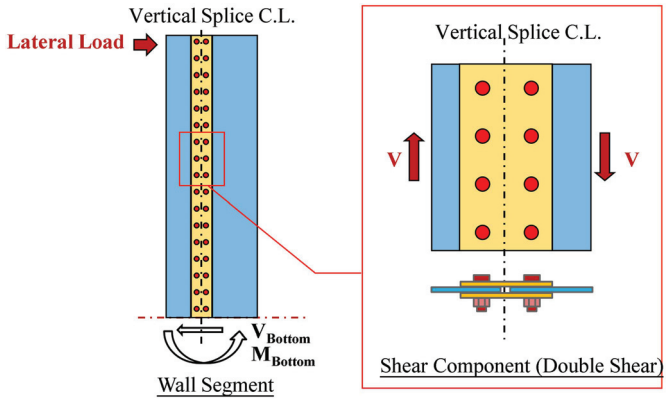

Fig. 2. Designed wall segment.

Table 1. Shear test specimens

Type	Case A (bearing)	Case B (slip-critical)	Case C (yielding)
Type 1 (blind bolts)	—	Specimens S3/S4	—
Type 2 (through bolts)	Specimens S1/S2	—	Specimens S5/S6

eccentricity, additional finite-element models were developed to investigate how increasing splice length can mitigate these effects. Also, using finite-element models considering longer walls segments more representative of bolted splices in C-SPW/CF, a proposed shear strength formula was developed to account for the combined effects of the bearing strength of steel and the shear strength of concrete.

Design of Component Specimens, Instrumentation, and Testing Protocol

Fig. 2 illustrates a corresponding wall segment subjected to story shear force and overturning moment due to lateral loads. A double shear connection is adopted to represent a segment of the wall's vertical splice, which is subjected to shear load from the splice's shear flow.

Shear Specimens

In the shear tests, the connection details vary to account for different fastener types used and desired governing limit states. Table 1 shows a summary of shear test specimens selected for the test program. As shown in Fig. 3, developed by Magnusson Klemencic Associates, there are two types of splice configurations considered in this case, namely, Type 1 - blind bolts and Type 2 - through rods with pipe sleeves. The designation Case A, B, and C is used to represent different governing limit states, respectively, bearing, slip-critical, and yield strength control. The three different types of

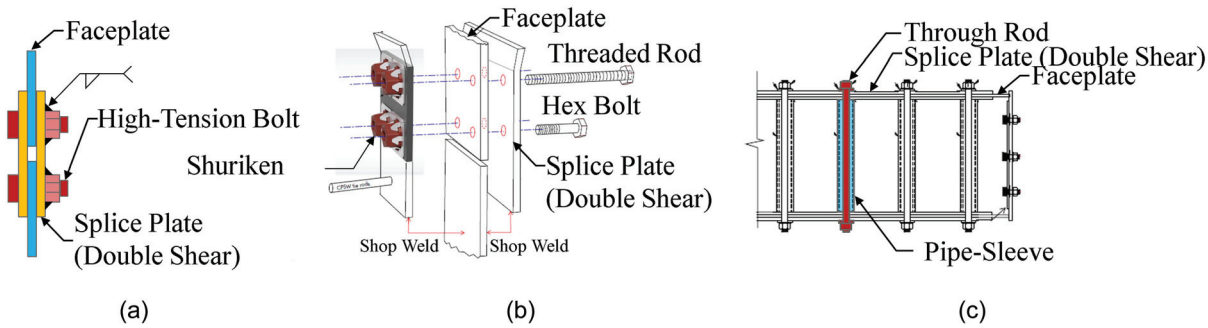

Fig. 3. Different types of bolts: (a) prewelded nuts; (b) shuriken; and (c) through rod with pipe sleeve.

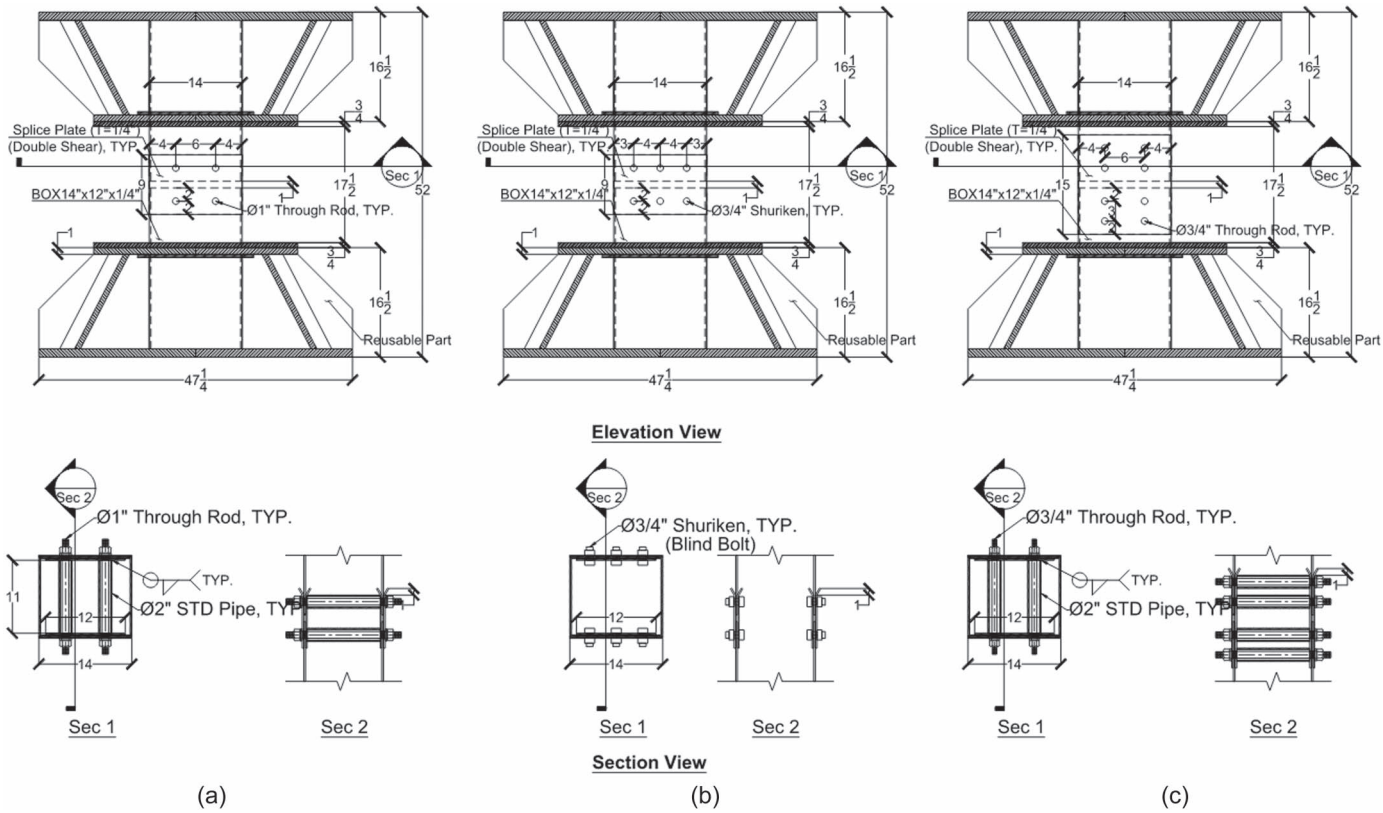

Fig. 4. List of shear specimens: (a) Specimens S1 and S2; (b) Specimens S3 and S4; and (c) Specimens S5 and S6.

connections were selected to represent different details considered by industry for applications of bolted splices in C-SPW/CF, while at the same time dimensioned/sized to investigate behavior of different limit states.

In shear, it is unescapable that the presence of concrete will allow the development of a diagonal compression strut acting simultaneously to the strength provided by the steel splice. To be able to separate the contribution of steel and concrete, testing included specimens without concrete in the splice region and comparable ones with concrete for which full composite action can develop. The steel-only specimens are designated as S1, S3, and S5, while those with concrete infill are Specimens S2, S4, and S6. Fig. 4 shows the six shear test specimens. The constant cross-section of the specimen, which consists of 6.4-mm-thick (0.25-in.) steel faceplates and splice plates, is the part tested in shear. Fig. 5 illustrates how specimens were inserted in a pantograph that was used in all shear tests to apply a condition of pure shear at midheight of the specimen (i.e., at the splice location). This pantograph already exists at the University at Buffalo and has been used successfully in prior research (Berman and Bruneau 2006; Kenarangi and Bruneau 2020). The maximum load that can be applied using this setup is 1,868 kN (420 kip). The pantograph consists of diagonal truss members connected to a center member and to the top loading and foundation beams by high-strength pin connections. Fig. 6

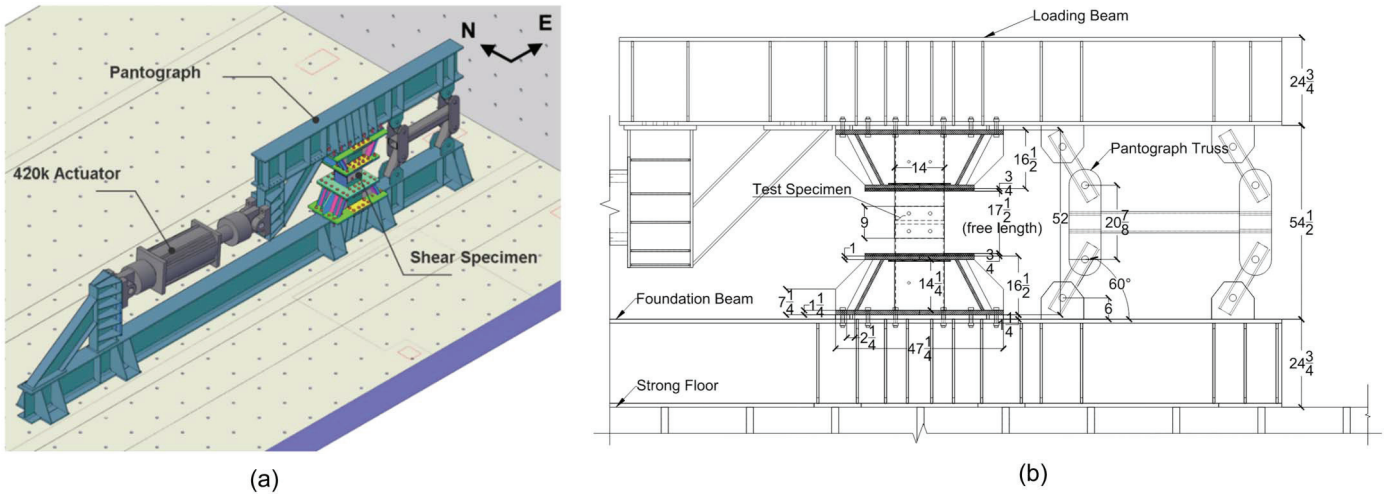

Fig. 5. Shear test setup: (a) 3D view; and (b) side view.

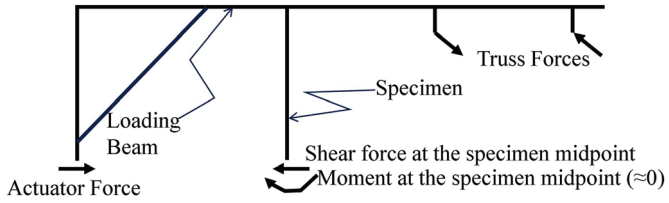

Fig. 6. Free body diagram of pantograph and specimen (cut at midpoint).

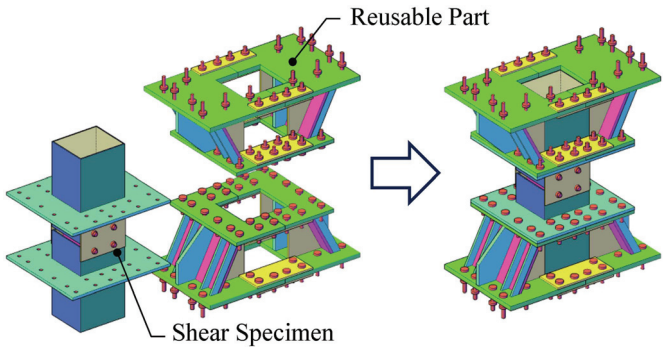

Fig. 7. Reusable parts for shear specimens.

Fig. 8. Test setup of shear component specimen.

provides a free-body diagram of the pantograph. This configuration allows horizontal translation of the top loading beam without resistance while preventing its rotation, thus eliminating axial force in the specimen and ensuring approximately equal specimen end moments, putting the specimen in double curvature, with shear and zero-moment at midheight of the specimen.

Note that a concept was developed to allow reuse of the steel framing the specimen outside of the splice region. As shown in Fig. 7, it consisted of bolted rectangular collars framing around the specimens, to keep their free length (the height of the specimen) short and therefore develop an ultimate behavior dominated by shear instead of flexure. This concept also allowed concrete to be cast into all of the specimens at the same time and in the lab, and made it possible to swap and sequentially test each composite specimen. Fig. 8 shows the test setup of a shear specimen in the laboratory.

The 444-mm (17.5-in.) free length was determined based on Specimen S5/S6, as shown in Fig. 4. A 2×2 bolt layout was chosen to achieve the gross section yielding strength of the steel faceplates. This resulted in a 381-mm (15-in.) splice plate height, with an additional 32-mm (1.25-in.) clearance at the top and bottom of the faceplates to ensure sufficient space for the splice plate to rotate without contacting the top and bottom fixture plates. The length of the reusable spaces was then designed to ensure that the trusses in the pantograph maintain reasonable angles between 30° and 60°.

The steel components of the shear specimens were fabricated in the shop, and their infill concrete was poured on the same day in the laboratory at the University at Buffalo. For the pretensioning process, all bolts for the shear specimens were either assembled using a torque gun or done by the fabricator. For Specimen S3, the turn-of-the-nut method was applied, rotating the nut 1/3 of a turn after snug tight. For Specimen S4, the bolts were pretensioned by the fabricator. The remaining specimens were assembled using a torque gun, applying a torque of approximately 400 ft-lb.

Material Properties and Limit States

A572 Gr. 50 steel was used in the construction of all specimens. All the 6.4-mm-thick (0.25 in.) steel plates used for the shear specimens were cut from the same sheet. Three coupon specimens were cut from the splice plate of Specimen S1, and all coupon specimens were tested under uniaxial tension. The average yield strength, F_y, for the steel plate was 440 MPa (63.9 ksi), and the average ultimate strength, F_u, for each coupon test was 503 MPa (72.9 ksi). For concrete, fifteen 152.4 mm × 304.8 mm (6 in. × 12 in.) cylinders were taken on the day of concrete pouring from the concrete batch used for the infill of the shear specimens. This large number of cylinders enabled periodic testing and monitoring of concrete strength over time. The corresponding concrete strength on the day of testing for composite Specimens S2, S4, and S6 were 21.4 MPa (3.1 ksi), 22.1 MPa (3.2 ksi), and 21.4 MPa (3.1 ksi), respectively.

The designation of Specimens S1/S2, S3/S4, and S5/S6 is used to represent different governing limit states: bearing strength, slip-critical, and yield strength control, respectively. Table 2 shows the design shear strength calculated per AISC-360 equations for each shear specimen under different limit states. In the table, "target load," or design shear strength, refers to the assumed shear force that the splice would have to be designed to resist over that segment of wall of a given length, where this length (equal to width of the specimen in the pantograph) is selected to be the same for all shear component test specimens. The term "sequence" is used to rank, from weakest to strongest, the strengths obtained considering various limit states for each wall segment. Lastly, the net section shear yielding strength ($0.6A_eF_y$) listed in Table 2 was provided as a reference and not used as a failure prediction.

For Specimens S1/S2 and S5/S6, the limit state of slip-critical resistance was ignored. In addition, although connection eccentricity would typically not be an issue in the long splices of walls, since the eccentricity of shear connection is unavoidable for the specimens considered here, bearing strength subjected to combined shear force and torsion in the system were also calculated using the elastic method from the AISC Steel Manual, but replacing bolt strength by bearing strength. These values are included in the table for comparison purposes.

Note that when establishing the hierarchy of limit states during design of the specimen, these eccentricities were neglected. Additionally, the instantaneous center of rotation method has not been used, as the intent in calculating eccentricities here is solely to give an indication of the consequence of eccentric loading on results, and as there would be no eccentricity effect in C-SPW/CF, as shown in later sections of this paper.

Table 2. Limit states for shear Specimens S1 to S6

Target loading V_u (kip)	S1/S2		S3/S4		S5/S6	
	175		142		268	
Limit states	Strength (kip)	Sequence	Strength (kip)	Sequence	Strength (kip)	Sequence
A. Slip-critical resistance (kip)	168	1	142	1	190	3
B. Net section yield ($0.6A_eF_y$) (kip)	225	5	218	5	235	4
C. Gross area yield ($0.6A_gF_y$) (kip)	268	8	268	8	268	7
D. Bearing capacity (kip)	175	4	197	4	263	5
E. Tear-out capacity (kip)	364	9	386	9	760	11
F. End tear-out & bearing (kip)	238	6	243	6	443	9
G. Net section rupture ($0.6A_eF_u$) (kip)	257	7	249	7	268	6
H. Bolt shear strength (kip)	531	11	445	11	594	10
I. Eccentric bearing capacity $2.4dtF_u$ (kip)	134	2	144	2	146	1
J. Eccentric bearing capacity $3.0dtF_u$ (kip)	168	3	180	3	183	2
K. Composite shear strength (kip)	406	10	406	10	406	8

Note: $F_y = 440$ MPa (63.9 ksi); $F_u = 503$ MPa (72.94 ksi); and 1 kip = 4.45 kN.

Instrumentation and Test Protocol

String potentiometers were used to measure the shear deformation and the vertical deformation of the specimens. As shown in Fig. 9, six string potentiometers were installed around the specimen. String potentiometers SP1 and SP2 were used to obtain the shear deformation (SP2–SP1) over the free length of the connection by measuring the displacement at the top and bottom of this free length of the specimen. String potentiometers SP3 to SP6 were used to measure the vertical movements between the plates at the end of the specimen's free length, as well as between the top and bottom of the reusable parts. In addition, four linear potentiometers (L1 to L4) were installed at four different levels on the specimen and reusable parts. Their purpose was to measure the relative movements between the pantograph and the reusable part, as well as between the reusable part and the connection part. No relative movement due to sliding was observed from the linear potentiometers during tests.

The testing protocol in Fig. 10 was proposed for the component specimens. Considering the description in Section 7.4.3.2 of the Pre-Standard for Performance-Based Wind Design (ASCE 2019), inelastic strain at 1.5 times the section yield should be limited to approximately 10 cycles. Therefore, 10 cycles were applied at this amplitude. For cycles below that amplitude, the target was to also apply a maximum of 10 cycles, up to the nominal strength ($1.0P_w$). Previous research by Kizilarslan and Bruneau (2023) subjected T-shaped composite plate shear walls to 500 cycles in the elastic range, without strength degradation after the first few cycles. In consultation with the Project Advisory Group, considering that 500 cycles in the previous research for a single specimen took over a week of continuous testing without any benefit beyond the first few cycles, in this study, a maximum of 10 cycles was chosen as an upper limit, provided that strength degradation has stabilized within these 10 cycles. For cycles above 1.5 times yield, the number of cycles applied followed an intent of a protocol similar to that specified in AISC-341. Beyond that, the intent was (1) for Specimens S1 to S4 to be still loaded with 10 cycles at each amplitude up to failure, to investigate the shear behavior beyond performance-based wind loads; and (2) for Specimens S5 and S6, because they were expected to reach their gross section shear yielding strength, to apply fewer subsequent cycles after reaching the nominal strength, following practices commonly used in conventional earthquake

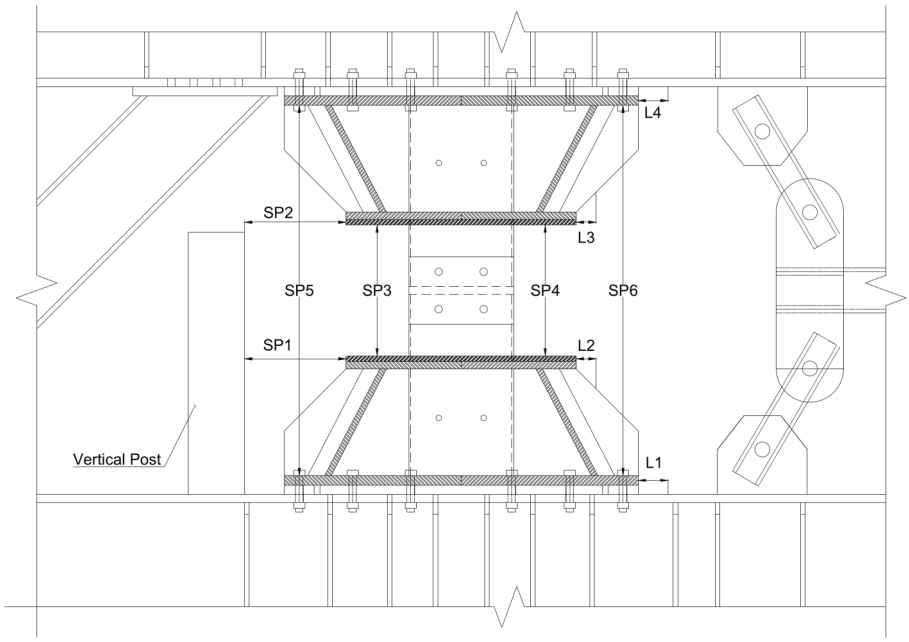

Fig. 9. String and linear potentiometers of shear specimens.

*Pw = design wind load

Phase	TYP. Wind	P.B. Wind
1	10 cycles @ 0.5Pw	10 cycles @ $0.5\gamma_y$
2	10 cycles @ 0.75Pw	10 cycles @ $0.75\gamma_y$
3	10 cycles @ 1.0Pw	10 cycles @ $1.0\gamma_y$
4	-	10 cycles @$1.5\gamma_y$
5	-	2 cycles @ $2.0\gamma_y$
6	-	2 cycles @ $3.0\gamma_y$
7	-	2 cycles @ $4.0\gamma_y$
8	-	2 cycles @ $5.0\gamma_y$

Keep increasing until failure

(a)

Phase	TYP. Wind	P.B. Wind/Seismic
1	10 cycles @ 0.5Pw	10 cycles @ $0.5\gamma_y$
2	10 cycles @ 0.75Pw	10 cycles @ $0.75\gamma_y$
3	10 cycles @ 1.0Pw	10 cycles @ $1.0\gamma_y$
4	-	10 cycles @$1.5\gamma_y$
5	-	2 cycles @ $2.0\gamma_y$
6	-	2 cycles @ $3.0\gamma_y$
7	-	2 cycles @ $4.0\gamma_y$
8	-	2 cycles @ $5.0\gamma_y$

Keep increasing until failure

(b)

Fig. 10. Original loading protocol for shear test: (a) for Specimens S1 to S4; and (b) for Specimens S5 to S6.

engineering. However, the loading protocols described earlier were slightly modified for each specimen based on observations while running the test. The original loading protocol specified running 10 cycles at 1.5 times the yield strain, followed by 2 cycles after the $1.5\varepsilon_y$. However, during testing, it was decided to extend the 10 cycles up to the bearing strength of $2.4dtF_u$. to observe possible strength degradation upon repeated cycling. Additionally, more than 2 cycles were performed beyond $2.4dtF_u$ to gain a more comprehensive understanding of the specimen's inelastic behavior. The updated loading protocols are listed in Table 3.

As the specimens were tested before the steel coupon tests, the target nominal strength (P_w) in Table 3 is based on assumed yield strength (R_yF_y) and tensile strength (R_uF_u) of 379 kPa (55 ksi) and 494 kPa (71.5 ksi), respectively. These assumed nominal strengths are lower than the actual material strengths shown in Table 2, where F_y and F_u are 440 MPa (63.86 ksi) and 503 MPa (72.94 ksi), respectively.

Test Observations and Results

Test Observations

Fig. 11 summarizes all test results of shear specimens, with the applied shear force versus shear deformation. Various aforementioned limit states are marked in the figure. Fig. 12 shows all shear specimens at the point of failure during testing, while Fig. 13 reveals the damage observed in the shear specimens after the splice plates were removed posttesting. More specifically, the following steps were followed:

- Specimen S1: During the Step 1 loading cycle, at an actuator force of 111 kN (25 kips) and a corresponding displacement of 2.5 mm (0.1 in.), the first sliding between the splice plates and faceplates was observed, accompanied by a loud bang when the actuator moved toward the positive peak displacement. More severe rotation of the splice plates can be observed in subsequent steps. The peak shear forces reached 933 kN (209.7 kip) in the positive direction during Step 6 and –818 kN (–184 kip) in the negative direction during Step 5, both exceeding the target nominal strength of 766 kN (172 kip), which corresponds to the bearing strength of $2.4dtF_u$. When the actuator reached the negative peak in Step 6, another loud bang was heard, followed by an abrupt drop in force due to connection failure. After this, the specimen was pulled further to a −127-mm (−5.0-in.) displacement in Step 7, resulting in noticeable tear-out damage.
- Specimen S2: During Step 1, evidence of sliding was observed, indicated by a reduced stiffness in the load-deformation curve at an actuator force of 133 kN (30 kip). However, this sliding was less significant compared to Specimen S1, as the concrete infill restricted the movement between the lower and upper parts of the specimen. No visible concrete damage was observed during the loading cycles up to the nominal strength level at Step 4. Starting from the loading cycles in Step 5, several pieces of concrete fell off from the sides. At Step 6, the shear force peaked at 1,134 kN (255 kip) in the positive direction and −988 kN

Table 3. Modified loading protocols during testing

Step	Disp. (in.) +	Disp. (in.) –	Force (kip) +	Force (kip) –	Cycles	Force Level
	(a) Modified loading protocol for Specimen S1					
0	0.00	0.00	0	0	—	—
1	0.47	0.53	43	43	10	$0.25P_w$
2	0.96	0.84	86	86	10	$0.5P_w$
3	1.26	1.19	129	129	10	$0.75P_w$
4	1.68	1.95	172	172	10	$1.0P_w$
5	2.20	2.50	185	190	5	—
6	2.90	3.20	209.7	184	—	Failure
7	—	5.00	—	—	—	Final
	(b) Modified loading protocol for Specimen S2					
0	0.00	0.00	0	0	—	—
1	0.12	0.13	43	43	10	$0.25P_w$
2	0.27	0.28	86	86	10	$0.5P_w$
3	0.45	0.50	129	129	10	$0.75P_w$
4	0.75	0.83	172	172	10	$1.0P_w$
5	1.05	1.16	219	199	5	—
6	1.50	1.70	255	222	5	—
7	2.00	2.30	251	220	5	—
8	2.50	2.80	251	175	4	—
9	3.00	3.30	216	160	1	Failure
	(c) Modified loading protocol for Specimen S3					
0	0.00	0.00	0	0	—	—
1	0.11	0.08	36	36	10	$0.25P_w$
2	0.21	0.19	72	72	10	$0.5P_w$
3	0.30	0.29	107	107	10	$0.75P_w$
4	0.42	0.53	143	143	10	$1.0P_w$
5	0.66	0.77	182	180	10	—
6	0.90	1.01	211	210	10	$2.4dtF_u$
7	1.14	1.25	220	216	5	—
8	1.48	1.59	234	231	5	$0.6A_gF_y$
9	1.92	2.03	244	240	5	$0.6A_eF_u$
10	2.46	2.57	249	242	5	—
11	2.70	—	224	—	—	Failure
12	4.00	—	—	—	—	Final

Table 3. (*Continued*.)

Step	Disp. (in.) +	Disp. (in.) −	Force (kip) +	Force (kip) −	Cycles	Force Level
	(d) Modified loading protocol for Specimen S4					
0	0.00	0.00	0	0	—	—
1	0.10	0.09	36	36	10	$0.25P_w$
2	0.20	0.18	72	72	10	$0.5P_w$
3	0.30	0.30	107	107	10	$0.75P_w$
4	0.46	0.42	143	143	10	$1.0P_w$
5	0.69	0.68	188	188	10	A_eF_y
6	0.92	0.94	247	236	10	$0.6A_eF_u$
7	1.15	1.20	282	271	5	—
8	1.48	1.56	313	300	5	—
9	1.91	2.02	305	292	5	—
10	2.44	2.58	276	246	4	Failure
	(e) Modified loading protocol for Specimen S5					
0	0.00	0.00	0	0	—	—
1	0.53	0.14	58	58	10	$0.25P_w$
2	1.09	0.67	116	116	10	$0.25P_w$
3	1.70	0.88	173	173	10	$0.5P_w$
4	2.14	1.53	231	231	10	$0.75P_w$
5	2.58	2.18	248	252	10	$2.4dtF_u$
6	3.02	2.83	252	258	10	—
7	3.46	3.48	252	222	2	Failure
	(f) Modified loading protocol for Specimen S6					
0	0.000	0.000	0	0	—	—
1	0.155	0.140	58	58	10	$0.25P_w$
2	0.320	0.310	116	116	10	$0.5P_w$
3	0.500	0.540	173	173	10	$0.75P_w$
4	0.750	0.900	231	231	10	$1.0P_w$
5	0.940	1.110	258	258	10	$2.4dtF_u$
6	1.130	1.320	286	272	5	—
7	1.320	1.530	295	274	5	—
8	1.610	1.840	308	285	5	—
9	2.000	2.250	312	289	5	—
10	2.490	—	269	—	—	Failure

Note: 1 in. = 25.4 mm; and 1 kip = 4.45 kN.

(−222 kip) in the negative directions, representing a 21% to 22% increase compared to Specimen S1. After Step 6, the applied force gradually decreased, the connection damage became more severe, and the rotation of the splice plate became quite noticeable. The condition of the connection at Step 9 showed that the through-rods had torn out of the faceplates. At this point, it was decided to terminate the test and return the actuator back to zero displacement. The test results of Specimens S1 and S2 indicate that both specimens achieved the shear strength necessary to develop the bearing strength of $2.4dtF_u$. As the bearing strength increased upon larger hole deformation, Specimen S2 was able to develop net section shear rupture strength ($0.6A_eF_u$) in the positive direction. Both specimens ultimately failed due to the increasing bearing deformation, which eventually caused tear-out at the bolt holes.

- Specimen S3: The first instance of sliding during testing was recorded in Step 4 when the applied forces increased to $1.00P_w$. A loud bang was heard due to the sliding between splice plates and faceplates when the actuator moved toward the negative direction. The peak force before sliding was −641 kN (−144 kip), which was close to the calculated slip-critical resistance of −630 kN (−141.53 kip). After sliding occurred, the rotation of splice plates became noticeable and progressively more severe. At Step 10, the applied forces reached peak values of 1,107 kN and −1,079 kN (249 kip and –242 kip) in the positive and negative directions, respectively. During Step 11, the applied force experienced a sudden drop when the load reached 994 kN (224 kip) and the displacement reached 68.6 mm (2.7 in.). The failure mechanism revealed that the top faceplates exhibit severe bearing deformations, while the bottom plates show a combined failure mechanism involving bearing failure and net section fracture.
- Specimen S4: No sliding or damage of concrete were observed during Steps 1 to 6. Concrete began to fall off during the loading cycles in Steps 7 and 8, with the applied load reaching peak values of 1,392 kN (313 kip) in the positive direction and −1,336 kN (−300 kip) in the negative direction, representing a 24% to 26% increase compared to Specimen S3. After this peak, the applied load gradually decreased with each subsequent cycle. The rotation of the splice plates became more noticeable, and concrete damage progressively worsened. The specimen ultimately failed during the third cycle in Step 10, and fractures on the bottom faceplates were observed. The test results for Specimens S3 and S4 show that the target limit state of slip-critical resistance was reached and exceeded in Specimen S3, while Specimen S4 did not exhibit a sliding plateau. Both specimens had a combined failure mechanism involving bearing failure and net section fracture. Specimen S3 developed net section shear rupture strength ($0.6A_eF_u$) before failure, with Specimen S4 achieved the gross section yielding strength ($0.6A_gF_y$) prior to failure.
- Specimen S5: The connection sliding was observed during Step 1 loading cycle when the applied force reached 212 kN (47.7 kip). The rotation of splice plates can be observed and became progressively more severe through successive loading cycles. In Step 6, the applied load reached its peak values of 1,120 kN (252 kip) in the positive direction and −1,148 kN (−258 kip) in the negative direction. On the third cycle of Step 7, the bottom faceplate fractured and moved sideways, as shown in Fig. 12(e). This resulted in significant bearing deformation and tearing out of the edge of the faceplate at this point. Therefore, the test was terminated. The failure mechanism revealed that the top faceplates exhibit severe bearing deformations and some fractures, while the bottom plates show a combined failure mechanism involving bearing failure and net section fracture.
- Specimen S6: No sliding or concrete damage was observed during the loading cycles from Steps 1 to 4. Starting from Step 5, some of the concrete on the side began to fall off, but no significant rotation of splice plates was observed. The rotation of the splice plates and the damage to the concrete became more severe during Steps 8 and 9, with the applied load reaching peak values of 1,387 kN (312 kip) in the positive direction and −1,285 kN (−289 kip) in the negative direction during Step 9, representing a 12% to 24% increase compared to Specimen S5. In Step 10 (final step), the applied loads reached 1,196 kN (269 kip), then dropped abruptly in the positive direction. The test results of Specimens S5 and S6 indicate that Specimen S5 reached a peak strength of 1,147 kN (258 kip), which was 3.7% below the target limit state of gross section shear yielding of 1,192 kN (268 kip). This discrepancy is likely due to eccentric loading effects, including shear and torsion. Specimen S6 was able to exceed the gross section yielding strength. Both specimens had a combined failure mechanism involving bearing failure and net section fracture.

Test Results and Summary

All the shear component specimens, for all the different connection details considered, were able to develop their calculated target loads. Specimens with splices that used blind bolts, or bolts with

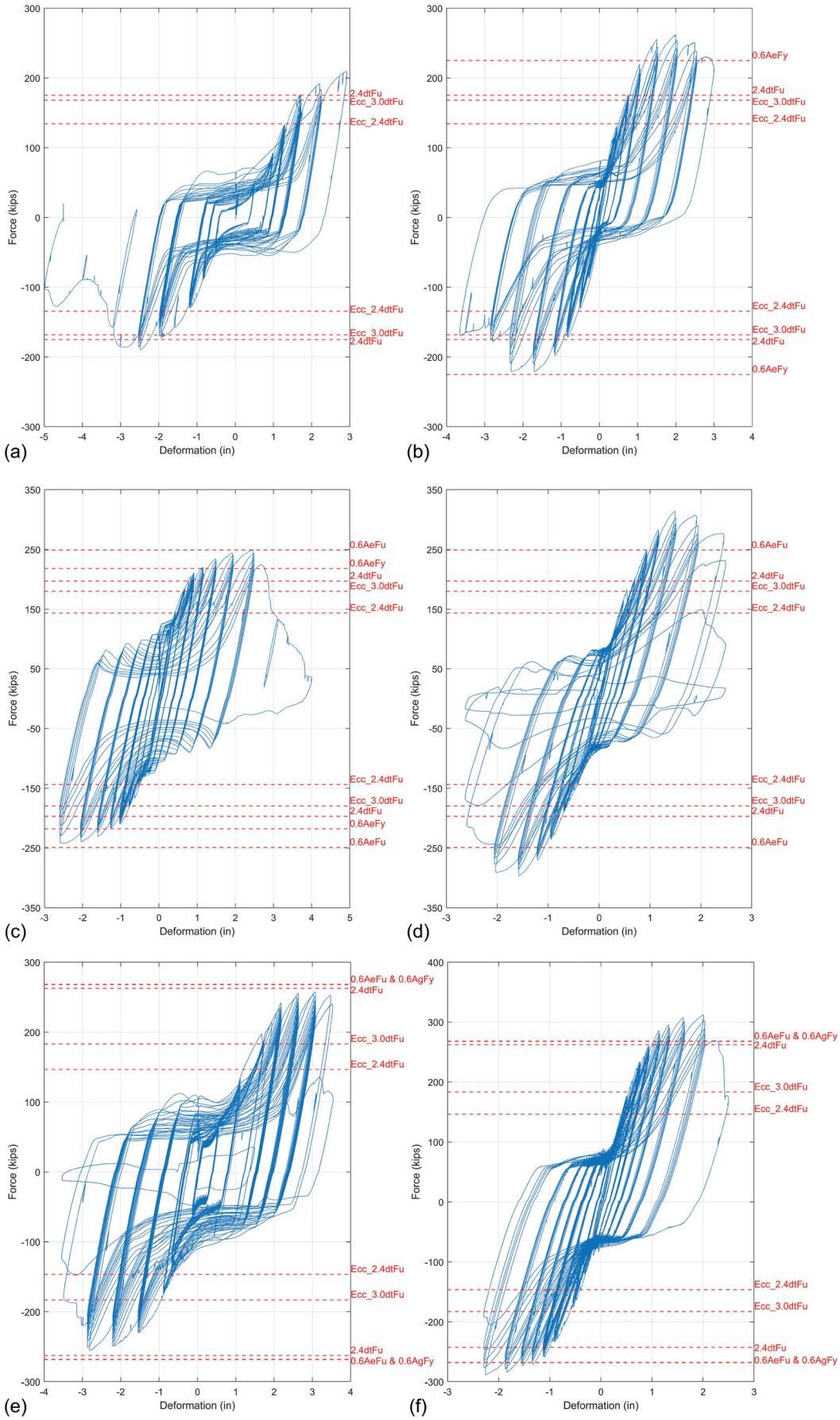

Fig. 11. Experimental results of shear specimens: (a) Specimen S1; (b) Specimen S2; (c) Specimen S3; (d) Specimen S4; (e) Specimen S5; and (f) Specimen S6.

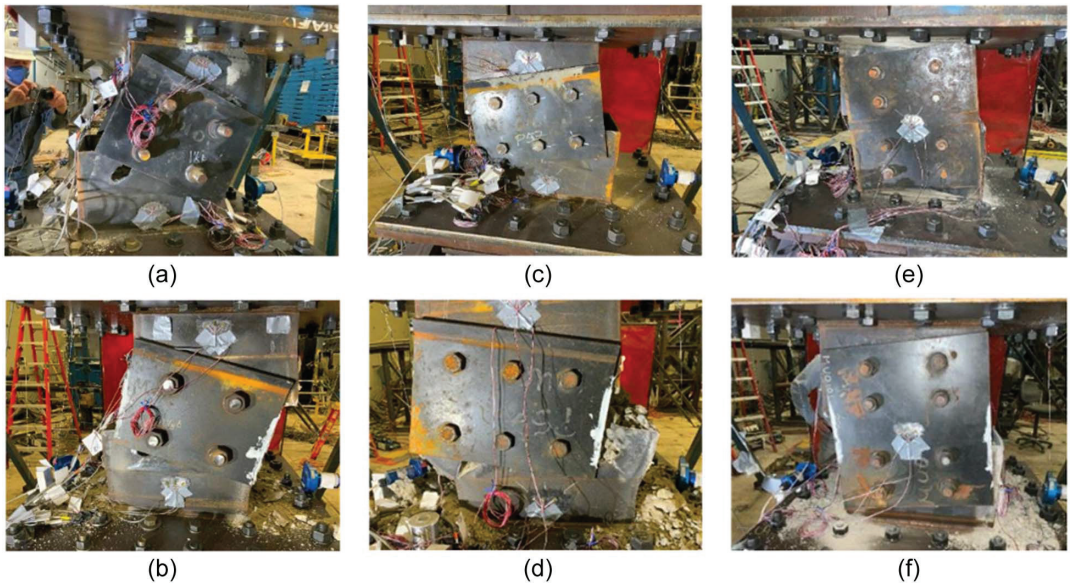

Fig. 12. Side views of shear specimen at failure: (a) Specimen S1 [Step 7, Disp. = −127 mm (−5 in.)]; (b) Specimen S2 [Step 9, Disp. = −83.82 mm (−3.3 in.)]; (c) Specimen S3 [Step 11, Disp. = 68.58 mm (2.7 in.)]; (d) Specimen S4 [Step 10, Disp. = 61.98 mm (2.44 in.)]; (e) Specimen S5 [Step 7, Disp. = 87.88 mm (3.46 in.)]; and (f) Specimen S6 [Step 10, Disp. = 63.25 mm (2.49 in.)].

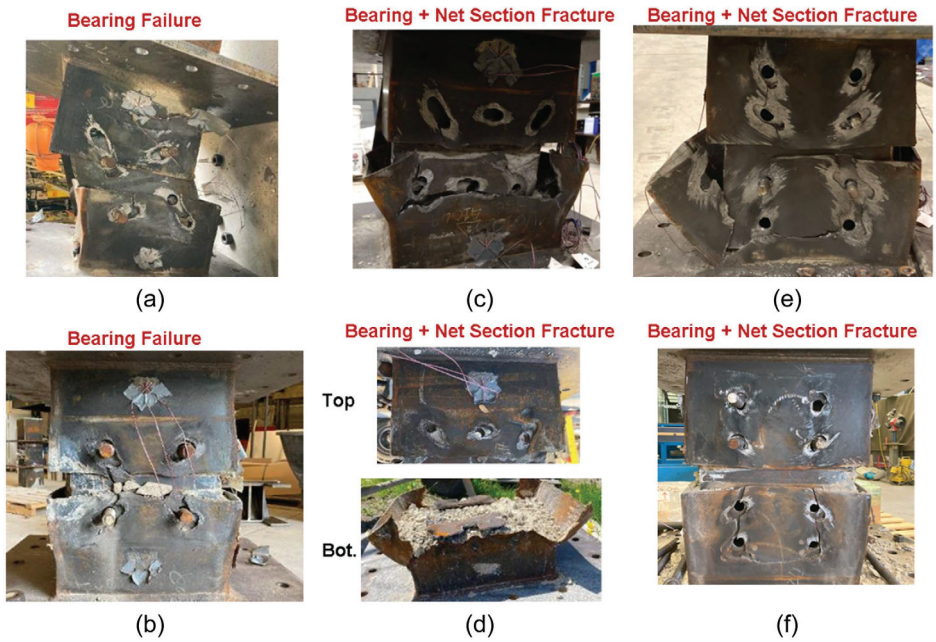

Fig. 13. Faceplates revealed after test: (a) Specimen S1; (b) Specimen S2; (c) Specimen S3; (d) Specimen S4; (e) Specimen S5; and (f) Specimen S6.

Shuriken inside the wall, generally developed their theoretical slip-critical strength, unlike those designed with threaded rods through pipe sleeves. All bearing strength results obtained in the test were developed with significant deformations. The following specific results were obtained:

- Positive and negative displacement amplitudes are unsymmetrical during the testing of shear specimens. The unsymmetrical displacement occurred because the shear specimens were tested with symmetric load targets below and up to the target load. After reaching the target load ($1.0P_w$), displacement was manually controlled by applying constant increments in both positive and negative directions. During testing, the specimen was subjected to large displacements in the direction where failure initially occurred to observe a clear failure mechanism. Therefore, Fig. 11 shows unsymmetrical behavior under large deformation.
- All shear specimens exhibited similar behavior. For the non-composite shear specimens, the sequence began with the initial sliding of the bolted connection, followed by bearing deformation of the bolts under torsional forces, ultimately leading to bearing failure or net section rupture. For the composite shear specimens, however, sliding only occurred after the concrete was crushed enough to create space for sliding.
- The composite sections were initially stiffer and reached peak force with significantly less sliding in the splice compared to

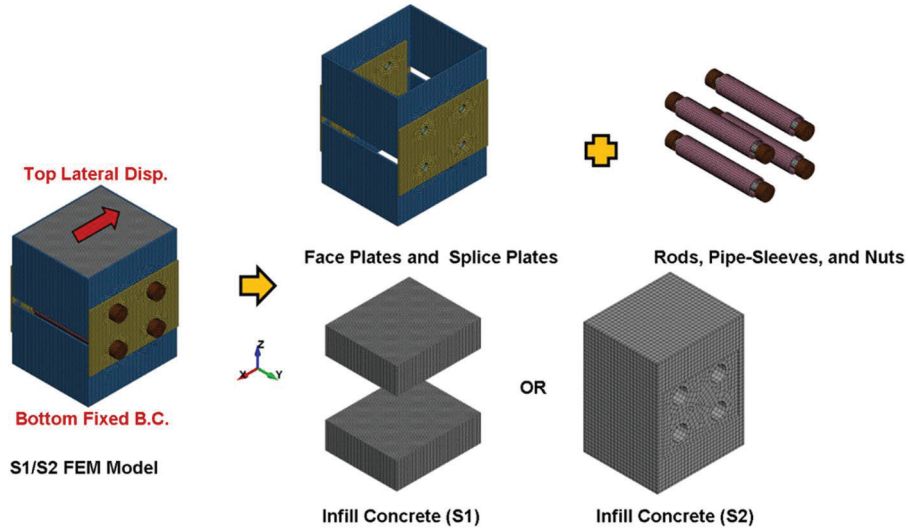

Fig. 14. Finite-element model of Specimens S1 and S2.

noncomposite sections. The peak shear strength of the composite section was typically sustained over larger deformations, whereas the strength of the noncomposite sections progressively increased with larger deformations up to failure. However, as deformations increased beyond 2.5 cm (1 in.), the strength of the composite sections progressively degraded to approach that of the noncomposite sections before failure. The results indicate that, ultimately, as the concrete severely cracked and crushed, its contribution to the shear strength decreased.

- In the shear component tests (S1 to S6), bearing strengths were calculated in the direction parallel to the splice. However, strength was also verified using the elastic method for eccentric connections, per the procedure in the AISC manual, which considers an eccentric bolt group to develop bearing strengths of $2.4dtF_u$ and $3.0dtF_u$, and all specimens were able to develop and exceed these strengths during the tests. Moreover, despite all composite and noncomposite specimens exceeding the shear strength necessary to develop a bearing strength of $2.4dtF_u$, in the direction parallel to the splice, diagonal deformation was observed in the bolt holes of the splice plates in all shear specimens, indicating a combined behavior of shear and torsion on the splices due to the fact that some flexure was unavoidably applied to the specimen simultaneously with the shear force.

Finite-Element Analysis of Shear Specimens

Finite-Element Model and Properties

Finite-element analysis of the shear Specimens S1 to S6 was conducted using LS-DYNA. Fig. 14 shows examples of the finite-element models for Specimens S1 and S2. The figure demonstrates various components of the assembled models and the reference coordinate system for the x-, y-, and z-directions. All steel (plates, bolts, etc.) was modeled using the *plastic_kinematic* (MAT_003) bilinear material model with kinematic hardening. The properties of the steel material used in the finite-element analyses are presented in Table 4. For concrete elements, the Winfrith concrete material model (MAT_085 in LS-DYNA) was used, as summarized in Table 5. The *automatic_surface_to_surface_mortar* contact model was used for all the contact interfaces, and a static interface friction coefficient of 0.3 was assigned. Bearing contact in LS-DYNA was modeled using a contact spring, as described in the LS-DYNA theory manual (Hallquist 2006), to develop the normal force. The sliding contact and friction behavior were represented by applying the friction coefficient to the normal force, generating the frictional force. Table 6 presents a summary of the pretension values used in the finite-element models. The table includes the diameter (d_b) and area (A_b) of bolts or through rods, the initial stress (prestress) and pretension force (T_b) of bolts or through rods, and the coefficient of friction (μ). The theoretical slip resistance (R_{theory}) can be calculated using the formula $T_b \times$ # of bolts $\times \mu \times 2$ (for double shear), as indicated in the table. Additionally, the table also includes the observed slip resistances from the tests (R_{test}).

Table 4. Material properties for steel

Part	E_s (ksi)	Poisson's ratio	F_y (ksi)	E_t (ksi)	β
Steel plates	29,000	0.3	63.9	66.0	0.0
Bolts/rods	29,000	0.3	120	221.2	0.0

Note: 1 ksi = 1,000 psi = 6.89 MPa.

Table 5. Material properties for concrete

Specimen	E_c (ksi)	Poisson's ratio	f'_c (psi)	f_t (psi)	FE	ASIZE
S1 to S6	3,122	0.2	3,000	300	0.0034	0.50

Note: 1 ksi = 1,000; and psi = 6.89 MPa. FE = fracture energy; and ASIZE = representative element size in the finite element mesh.

Table 6. Prestress value used in finite element models

Specimen	d_b (in.)	A_b (in.^{2})	Prestress (ksi)	T_b (kip)	# of bolts	μ	R_{theory} (kip)	R_{test} (kip)
S1	1	0.79	52.5	41.2	4	0.30	99.0	40
S2	1	0.79	52.5	41.2	4	0.30	99.0	—
S3	0.75	0.44	52.5	23.2	6	0.30	83.5	144
S4	0.75	0.44	52.5	23.2	6	0.30	83.5	—
S5	0.75	0.44	52.5	23.2	8	0.30	111.3	48
S6	0.75	0.44	52.5	23.2	8	0.30	111.3	—

Note: 1 in. = 25.4 mm; 1 kip = 4.45kN; and 1 ksi = 6.89 MPa.

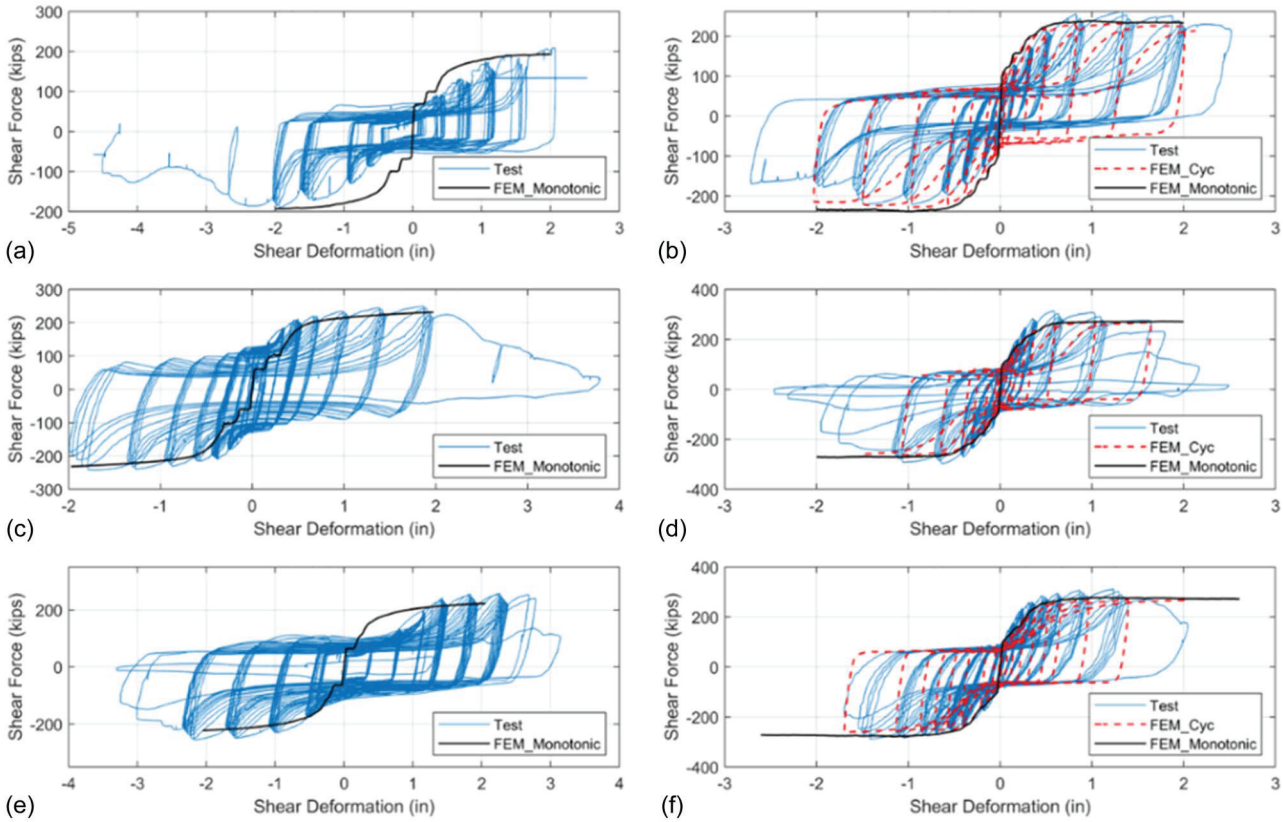

Fig. 15. Finite-element analysis results of shear specimens.

Finite-Element Analysis Results

Fig. 15 summarizes all finite-element analysis results compared with the corresponding test results for shear specimens, in terms of shear force versus shear deformation. Monotonic pushover analyses were conducted for all specimens, while cyclic loading analyses were applied to composite Specimens S2, S4, and S6. Fig. 16 shows the von Mises stresses of the faceplates during cyclic loading in Specimen S2. Five arbitrary points were selected to demonstrate the distribution of stress and deformation of the faceplates. The combined shear and eccentric torsion behaviors contributing to the hole deformation were captured in the model, representing the bearing behavior observed during testing.

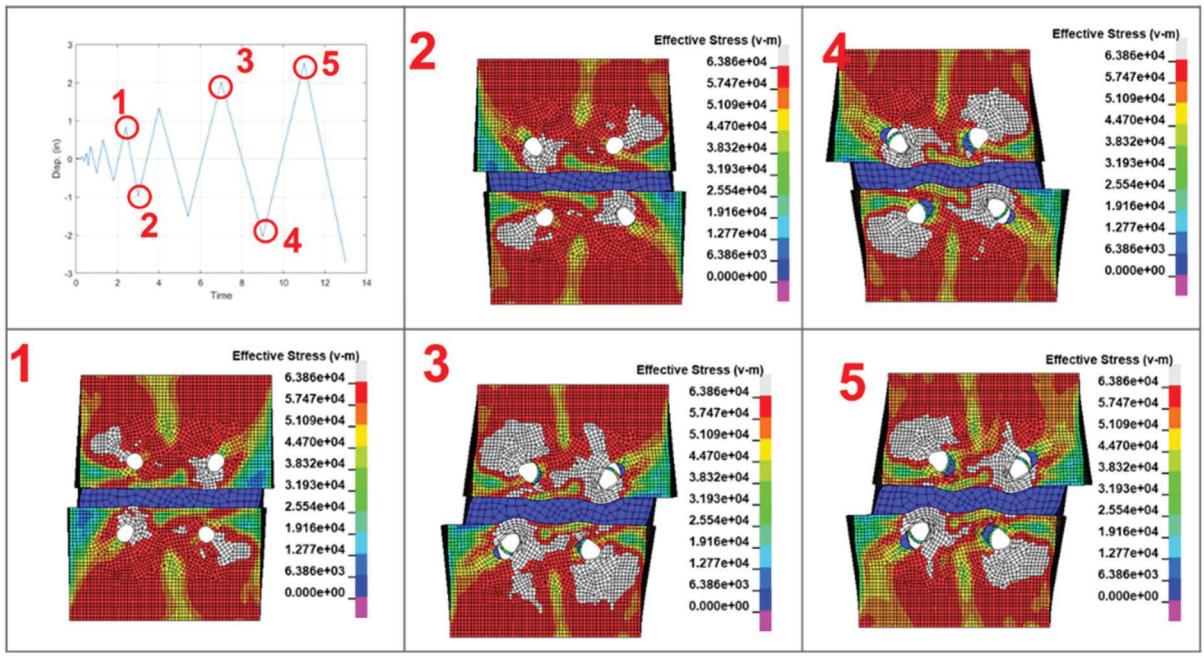

Fig. 16. Finite-element analysis results of Specimen S2.

Table 7. Comparison of peak shear forces of shear specimens

Specimen	V_{Test+} (kip)	V_{Test-} (kip)	V_{FEM} (kip)	V_{FEM}/V_{Test+}	V_{FEM}/V_{test-}
S1	210	184	194	0.93	1.05
S2	255	222	240	0.94	1.08
S3	249	242	231	0.93	0.96
S4	313	300	270	0.86	0.90
S5	252	258	224	0.89	0.87
S6	312	289	278	0.89	0.96

Note: 1 kip = 4.45 kN.

Table 7 summarizes the analysis results, highlighting peak shear forces in comparison to the corresponding test results. In the table, V_{FEM} denotes the peak shear forces obtained from the monotonic finite-element analysis, and V_{Test+} and V_{Test+} denote the peak shear force obtained from tests in the positive and negative directions, respectively. The results indicate that the peak shear forces predicted by the finite-element models demonstrate an accuracy range of −14% to 8% when compared to the test results across all specimens. The contribution of shear strength provided by concrete was found to be 25% to 31% of the total shear strength at peak shear strength of the composite shear specimens. This was achieved by cutting a cross-section at the middle of the finite-element model and isolating forces acting on the steel and concrete components separately.

Fig. 17 shows a comparison of shear strengths obtained from the S1 and S2 finite-element models. The peak shear strengths for S1 and S2 are 863 kN (194 kip) and 1,068 kN (240 kip), respectively. By subtracting the shear strength of S1 from S2 over the entire deformation range, the shear strength provided by the concrete component can be somewhat inferred, and is labeled "S2-S1" in Fig. 17(a). The S2-S1 shear strength reaches a peak strength of 445 kN (100 kip) at a shear deformation of 8.9 mm (0.35 in.), and it decreases to 200 kN (45 kip) at a shear deformation of 50.8 mm (2.0 in.). Finally, the shear strength of concrete obtained from the S2 finite-element model is compared with the S2-S1 shear strength as shown in Fig. 17(b). Note that models S1 and S2 do not exhibit perfect synchronization of their behavior. For example, the two models experienced sliding at different deformation levels. Therefore, using the S2-S1 method to calculate the contribution of concrete to total strength may lead to inaccuracies.

Finite-Element Analysis of Wall Case Scenarios

Finite-Element Model and Properties

In this section, longer walls with bolted splices are examined to investigate the behavior of connections governed by shear while minimizing the influence of localized end-effects. Fig. 18 show four shear models (W1 to W4) constructed in LS-DYNA, and all these models share the same properties as the shear specimens S1 to S6. Table 8 provides the corresponding geometries of these models. The table compares the eccentricity ratios, representing the ratio of eccentric bearing strength ($Ecc.\ 2.4dtF_u$) to noneccentric (pure shear) bearing strength ($2.4dtF_u$) for Models W1 to W4. For Models W3 and W4, the ratios are 0.94 and 0.96, which are close to 1.0, representing the condition in a wall case scenario where the impact of eccentricity is negligible.

Finite-Element Analysis Results

Fig. 19 shows the shear strength per unit length of walls, including total shear strength V_T, steel shear strength V_S, and concrete shear strength V_C, for Models W1 to W4. As shown in the figure, the shear strengths per unit length increase for the longer walls as the effect of eccentricity diminishes and converge in Models W3 and W4 for cases where the eccentricity ratio is close to 1. This behavior is observed for the total strength and the steel shear strength per unit length, but not as markedly for the concrete shear strength per unit length.

The concrete shear strength specified for special structural walls in ACI 318-19 (ACI 2019) equation 18.10.4.1 was adopted here to compare with the concrete shear strength obtained in the shear models as shown below:

$$V_c = \alpha_c \lambda \sqrt{f'_c} A_{cv} \tag{1}$$

where $\alpha_c = 3$ for H/B ≤ 1.5 and $\alpha_c = 2$ for H/B ≥ 2, $\lambda = 0.75$ for lightweight concrete, and $\lambda = 1$ for normal-weight concrete, and A_{cv} is the gross area of the concrete section bounded by web thickness and length of the section in the direction of shear force. H/B is the aspect ratio of the wall, where H denotes wall height and B denotes wall length in the shear direction.

A further analysis was conducted based on Model W4, focusing solely on the center core of Model W4 to eliminate the edge effects

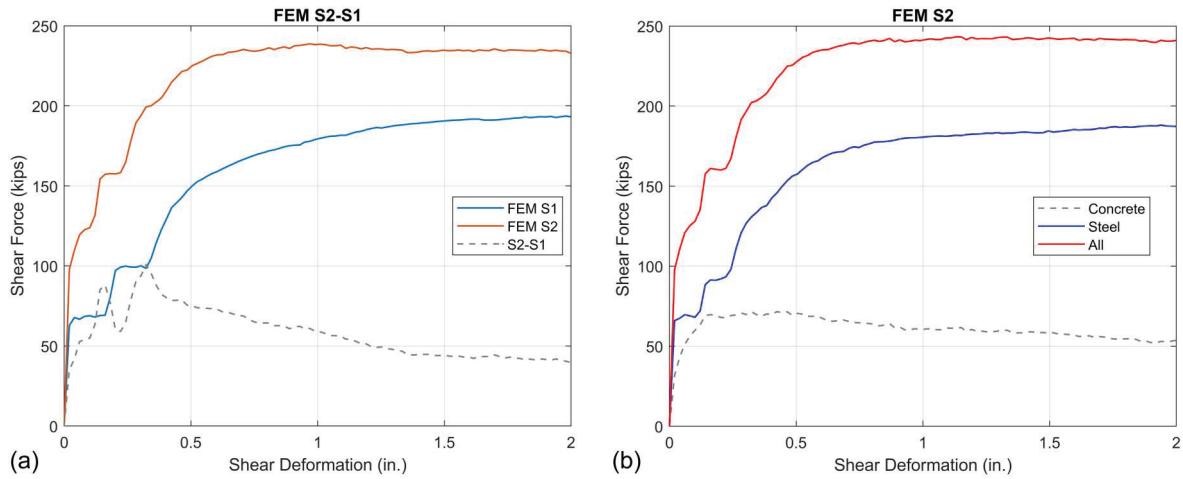

Fig. 17. Comparison of shear strengths between S1 and S2 finite-element models: (a) V_c obtained from S2-S1; and (b) V_c obtained from S2.

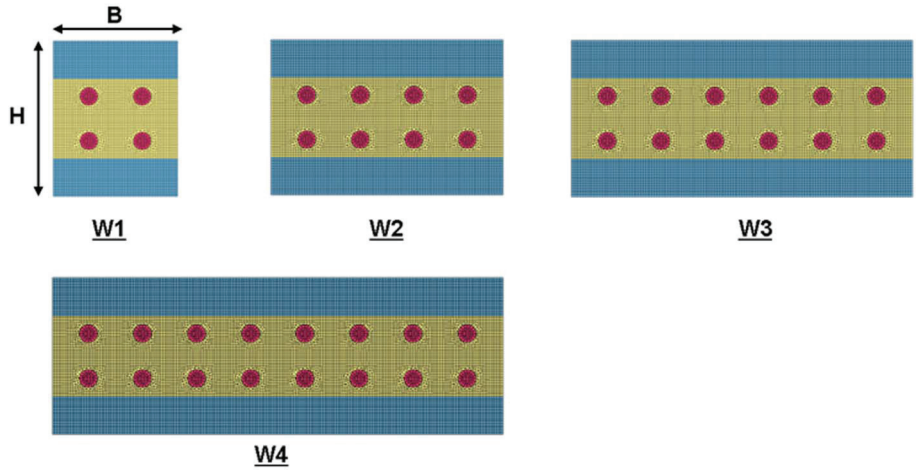

Fig. 18. Finite-element models of W1 to W4.

Table 8. Geometries and eccentricity ratio in Models W1 to W4

Parameter	W1	W2	W3	W4
Width B (in.)	14	26	38	50
Thickness T (in.)	12	12	12	12
Height H (in.)	17.5	17.5	17.5	17.5
B/T	1.2	2.2	3.2	4.2
B/H	0.8	1.5	2.2	2.9
$2.4dtF_u$ (kip)	175	350	525	700
Ecc. $2.4dtF_u$ (kip)	134	313	495	675
Eccentricity ratio	0.77	0.89	0.94	0.96

Note: 1 in. = 25.4 mm; and 1 kip = 4.45 kN.

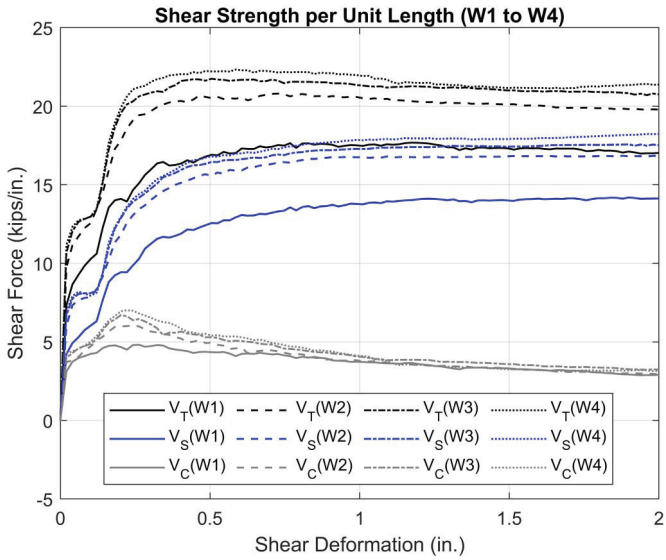

Fig. 19. Unit length shear strength versus shear deformation (Models W1 to W4).

caused by the cap plates. This condition was labeled as "Model W4_Core," representing the wall scenario without the influence of edge cap plates. Fig. 20 illustrates the comparison between W4 and W4_Core in LS-DYNA, while Fig. 21 shows the load-deformation curve of W4_Core obtained from finite-element analysis. The

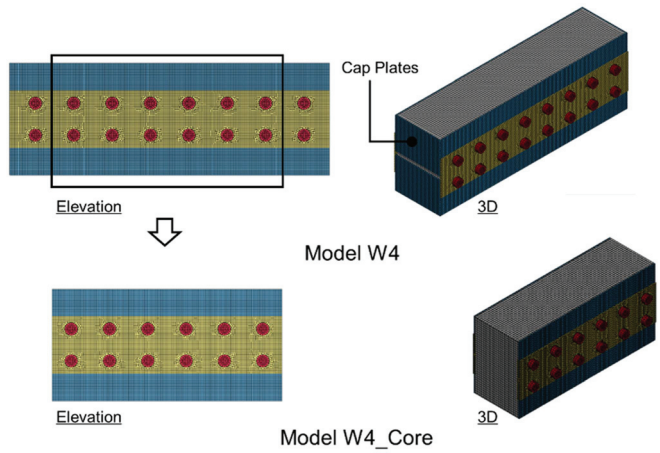

Fig. 20. Finite-element model of specimens W4 and W4_Core.

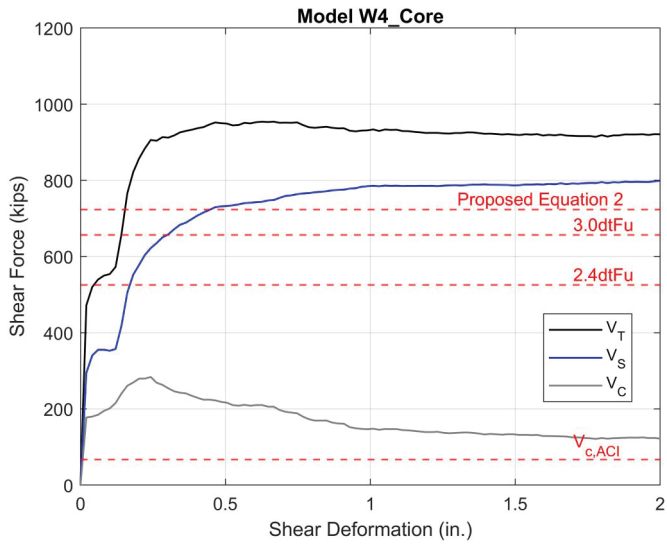

Fig. 21. Finite-element results of load-deformation curve of Model W4_Core.

Table 9. Shear strength per unit length comparison between Models W4 and W4_Core

Model	$V_{T,\max}$ (k/in.)	$V_{S,\max}$ (k/in.)	$V_{C,\max}$ (k/in.)	$V_{C,residual}$ (k/in.)	$V_{C,ACI}$ (k/in.)	$V_{2.4dtFu}$ (k/in.)	$V_{3.0dtFu}$ (k/in.)
W4	22.34	18.23	7.02	3.15	1.97	14.00	17.51
W4_Core	28.06	23.50	8.35	3.59	1.97	15.45	19.31

Note: 1 kip = 4.45 kN.

Table 10. Comparison of Eq. (2) and test specimens

Specimen	Test+ (kip)	Test-(kip)	Test+/Eq. (2)	Test-/Eq. (2)
S1	209.7	184.0	—	—
S2	255.0	222.0	1.33	1.16
S3	249.0	242.0	—	—
S4	313.0	300.0	1.47	1.41
S5	252.0	258.0	—	—
S6	312.0	289.0	1.12	1.04

Note: 1 kip = 4.45 kN.

figure also marks the bearing strength of $2.4dtF_u$ and the ACI concrete shear strength mentioned earlier.

Table 9 summarizes the shear strength per unit length of the total, steel, and concrete components in Models W4 and W4_Core, along with the corresponding shear strength per unit length calculated using the bearing strength of $2.4dtF_u$ and $3.0dtF_u$, and the ACI concrete shear strength equations. The results indicates that, for walls where the eccentricity of bolt group is less significant, the steel shear strength V_s can reach and exceed the bearing strength of $3.0dtF_u$ calculated parallel to the splice direction. However, for V_s to reach $3.0dtF_u$, it requires bolt holes to develop large deformations. Controlling the bearing strength to $2.4dtF_u$ allows for the shear deformation to be kept below 5.1 mm (0.2 in.) (refer to Fig. 21), helping to minimize the deformation of the connection for high-rise buildings. Therefore, it is recommended to keep the design steel shear strength at $2.4dtF_u$. In addition, the contribution of concrete, V_c, to the total shear strength can reach and exceed the shear strength value given by ACI 318-19 equation 18.10.4.1. Consequently, when the bearing strength is the governing limit state for steel, the nominal shear strength V_n of C-PSW/CF with a bolted connection can be conservatively obtained combining the shear strength of steel and concrete, expressed as follows:

$$V_n = V_s + V_c = 2.4dtF_u + \alpha_c \lambda \sqrt{f'_c} A_{cv} \quad (2)$$

Table 10 provides a comparison between the peak forces obtained from tested composite specimens and the proposed Eq. (2). Note that the test specimens have a width of only 355.6 mm (14 in.), which amplifies the impact of eccentricity. Even under this condition, Eq. (2) still delivers conservative results for steel-composite members having bolted splices.

Summary and Conclusions

The experimental observations and results indicate that all splice details examined successfully achieved the nominal strength calculated using the current AISC equations for bolted steel connections in shear. Finite-element models with monotonic and cyclic loading analysis accurately captured the test results, with peak strength comparisons ranging from −14% to 8% accuracy. In addition, longer walls with bolted connections were examined to investigate shear connections where eccentricity of the bolt group is not significant. A proposed equation combining the bearing strength of $2.4dtF_u$ and the ACI concrete shear strength equation 18.10.4.1 was developed to provide a conservative approach for estimating the shear strength of C-PSW/CF bolted splices. Overall, all analyses conducted validated the design equations used to calculate the strength of bolted C-PSW/CF splices in shear.

Data Availability Statement

Some or all data, models, or code that support the findings of this study are available from the corresponding author upon reasonable request.

Acknowledgments

This research was supported by the Charles Pankow Foundation (CPF), the American Institute of Steel Construction (AISC), the MKA Foundation, and Atlas Tube/Zekelman through CPF research grant #02-21. All opinions, findings, conclusions, and recommendations presented in this paper are those of the authors and do not necessarily reflect the view of the sponsors. The researchers are also grateful for the technical guidance of its Project Advisory Group members (Glenn Bell, National Institute of Standards and Technology; Ron Klemencic, Chairman and CEO, Magnusson Klemencic Associates; Jim Malley Senior Principal with Degenkolb Engineers; Rafael Sabelli, Principal and Director of Seismic Design, Walter P. Moore; Devin Huber, Director of Research at AISC; and Christopher Raebel and Larry Kruth current and former Vice President, AISC).

Author Contributions

Jia-Hau Liu: Writing – original draft. Michel Bruneau: Writing – review and editing.

References

ACI (American Concrete Institute). 2019. *Building code requirements for structural concrete (ACI 318-19) and commentary*. Farmington Hills, MI: ACI.

Agrawal, S. 2020. *Seismic design coefficients for composite plate shear walls—Concrete filled (C-PSW/CF)*. West Lafayette, IN: Purdue Univ.

AISC. 2022a. *Seismic provisions for structural steel buildings*. AISC 341-22. Chicago: AISC.

AISC. 2022b. *Specification for structural steel buildings*. AISC 360-22. Chicago: AISC.

Alzeni, Y. 2014. *Cyclic inelastic behavior of concrete filled sandwich panel walls subjected to in-plane flexure*. Buffalo, NY: State Univ. of New York at Buffalo.

Alzeni, Y., and M. Bruneau. 2017. "In-plane cyclic testing of concrete-filled sandwich steel panel walls with and without boundary elements." *J. Struct. Eng.* 143 (9): 04017115. https://doi.org/10.1061/(ASCE)ST.1943-541X.0001791.

ASCE. 2019. *Prestandard for performance-based wind design*. Reston, VA: ASCE.

ASCE. 2022. *Minimum design loads and associated criteria for buildings and other structures*. ASCE 7-22. Reston, VA: ASCE.

Berman, J. W., and M. Bruneau. 2006. *Further development of tubular eccentrically braced frame links for the seismic retrofit of braced steel truss bridge piers*. Buffalo, NY: Univ. at Buffalo, State Univ. of New York.

Brown, J. D., D. J. Lubitz, Y. C. Cekov, K. H. Frank, and P. B. Keating. 2007. *Evaluation of influence of hole making upon the performance of structural steel plates and connections*. Rep. No. FHWA/TX-07/0-4624-1. Austin, TX: Univ. of Texas at Austin.

Frank, K. H., and J. A. Yura. 1981. *An experimental study of bolted shear connections*. Washington, DC: DOT, Federal Highway Association.
Hallquist, J. O. 2006. *LS-DYNA® theory manual*. Livermore, CA: Livermore Software Technology Corporation.
Kenarangi, H., and M. Bruneau. 2020. "Shear strength of composite circular reinforced concrete–filled steel tubes." *J. Struct. Eng.* 146 (1): 04019180. https://doi.org/10.1061/(ASCE)ST.1943-541X.0002456.
Kim, D. K., and C. H. Lee. 2020. "Generalized load deformation relationship for bearing-type single-bolted connections." *J. Struct. Eng.* 146 (7): 04020116. https://doi.org/10.1061/(ASCE)ST.1943-541X.0002640.
Kim, H. J., and J. A. Yura. 1996. "The effect of end distance on the bearing strength of bolted connections." Doctoral dissertation, Dept. of Civil Engineering, Univ. of Texas at Austin.
Kizilarslan, E. 2021. *Experimental and analytical inelastic behavior of C- and T-shaped composite plate shear walls/concrete-filled (C-PSW/CF)*. Buffalo, NY: State Univ. of New York at Buffalo.
Kizilarslan, E., and M. Bruneau. 2021. "Hysteretic behavior of repaired C-shaped concrete filled-composite plate shear walls (C-PSW/CF)." *Eng. Struct.* 241 (Aug): 112410. https://doi.org/10.1016/j.engstruct.2021.112410.
Kizilarslan, E., and M. Bruneau. 2023. "Cyclic behavior of T-shaped composite plate shear walls–concrete filled." *J. Struct. Eng.* 149 (8): 04023102. https://doi.org/10.1061/JSENDH.STENG-11693.
Kulak, G. L., J. W. Fisher, and J. H. A. Struik. 1987. *Guide to design criteria for bolted and riveted joints*. Chicago: AISC.
Lewis, B. E., and F. J. Zwememan. 1996. *Edge distance, spacing, and bearing in bolted connections*. Stillwater, OK: Oklahoma State Univ.
Može, P. 2018. "Bearing strength at bolt holes in connections with large end distance and bolt pitch." *J. Constr. Steel Res.* 147 (Aug): 132–144. https://doi.org/10.1016/j.jcsr.2018.04.006.
Sener, K. C., and A. H. Varma. 2014. "Steel-plate composite walls: Experimental database and design for out-of-plane shear." *J. Constr. Steel Res.* 100 (Sep): 197–210. https://doi.org/10.1016/j.jcsr.2014.04.014.
Shafaei, S., A. H. Varma, J. Seo, and R. Klemencic. 2021. "Cyclic lateral loading behavior of composite plate shear walls/concrete filled." *J. Struct. Eng.* 147 (10): 04021145. https://doi.org/10.1061/(ASCE)ST.1943-541X.0003091.
Varma, A. H., S. R. Malushte, K. Sener, and Z. Lai. 2014. "Steel-plate composite (SC) walls for safety related nuclear facilities: Design for in-plane and out-of-plane demands." *Nucl. Eng. Des.* 269 (Apr): 240–249. https://doi.org/10.1016/j.nucengdes.2013.09.019.